Abstract We overview methods of THz-wave generation using frequency down-conversion in GaAs with periodically-inverted crystalline orientation. First, we compare different nonlinear-optical materials suitable for THz generation, analyze THz generation process in quasi-phase-matched crystals and consider theoretical limits of optical-to-THz conversion. Then, we review single-pass optical rectification experiments with femtosecond pump pulses, performed in periodically-inverted GaAs, where monochromatic THz output tunable in the range 0.9–3 THz was produced. Finally, we describe a novel approach to create a compact highly efficient tunable (0.5–3.5 THz) room temperature monochromatic THz source, based on the concept of intracavity THz generation via resonantly-enhanced difference frequency mixing. This approach allowed generating of 1 mW of average THz power, potentially scalable to 10–100 mW.

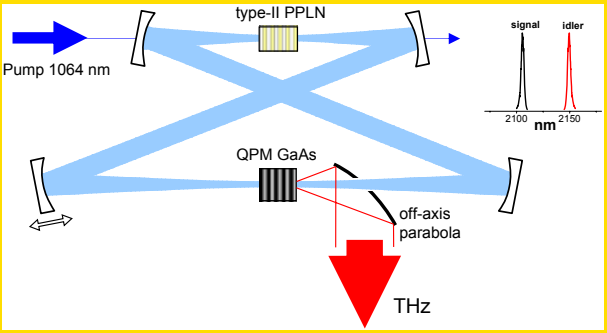

Conceptual scheme of resonantly-enhanced THz-wave generation. Near-degenerate doubly-resonant PPLN optical parametric oscillator produces two closely spaced 'signal' and 'idler' waves near 2 µm. THz output is produced at the beat frequency between these two waves, via frequency mixing in periodically-inverted GaAs.

Optical THz-wave generation with periodically-inverted GaAs

Konstantin L. Vodopyanov

Edward L. Ginzton Laboratory, Stanford University, Stanford, CA 94305, USA

Received: 23 October 2007, Revised: 5 December 2007, Accepted: 6 December 2007
Published online: 29 January 2008

Key words: terahertz; T-ray; frequency down-conversion; quasi-phase matching; gallium arsenide; optical parametric oscillator; synchronous pumping

PACS: 42.65.Lm, 42.70.Nq, 42.65.Yj, 42.72.Ai, 07.57.Hm

1. Introduction

There is a colossal potential for exploiting terahertz waves (1 THz = 10^{12} Hz, λ = 300 µm) in the fields extending far beyond the realms of their traditional use, like astronomy, study of Earth's atmosphere, high-resolution spectroscopy and plasma diagnostics. These new applications emerged in the last two decades and encompass 'friendly X-rays' real-time imaging (THz radiation experiences, in many occasions, much smaller scattering than the optical, and thus can penetrate many materials; yet the photon energy is too small to do any harm to living organisms), sensing and spectroscopic imaging by means of rotational-vibrational spectroscopy, because of extreme richness of absorption 'fingerprints' in the THz range, biomedical imaging (identifying cancers, particularly skin cancer), pharmaceutical industry (classifying molecular polymorphs), as well as broadband wireless communication [1]. Another emerging field is nonlinear interactions of THz waves with matter and nonlinear terahertz spectroscopy [2–4].

Regardless of a great variety of techniques for generating THz radiation [5], none of them provides a THz source which is simultaneously (i) compact, (ii) highly efficient, (iii) broadly tunable (octave or more), and (iv) works at room temperature. THz sources based on nonlinear optical effects, in particular those using $\chi^{(2)}$ nonlinearity, such as difference frequency generation (DFG), optical rectification, and optical parametric oscillation (OPO) are very

e-mail: Dr. Konstantin L. Vodopyanov: vodopyan@stanford.edu

appealing because they can capitalize on swift progress of diode-pumped lasers, in particular fiber lasers, which would allow making a THz system very compact. Another advantage is power scalability: unlike photomixers and dipole photoantennas [5], nonlinear optical sources do not suffer from saturation of THz output power and typically show quadratic dependence of the output vs. pump power. It should be mentioned that THz radiation can also be produced from optical radiation using $\chi^{(3)}$ nonlinearity: intense THz pulses were generated via four-wave rectification process in laser-created plasma in ambient air [6, 7].

In this paper, we briefly review different techniques of THz generation using $\chi^{(2)}$ processes, including quasi-phase-matched interactions, make comparison of linear and nonlinear properties of crystals suitable for THz-wave generation, consider theoretical limits of optical-to-THz conversion, and review optical rectification experiments performed with periodically-inverted GaAs. Finally, we will describe and review first experimental results on a new approach to optical THz-wave generation using periodically-inverted GaAs. This approach is based on frequency mixing of two resonantly-enhanced optical fields inside a cavity. We will also discuss recycling of optical photons via cascaded process, which makes it possible to substantially surpass Manley-Rowe conversion limit.

2. Optical THz-wave generation in nonlinear crystals

2.1. Frequency conversion using DFG and OPO

Generation of THz waves by difference frequency mixing using laser radiation and a nonlinear crystal was first performed by Zernike and Berman in quartz crystal inside the cavity of a ruby laser as early as in 1965 [8]. Later, tunable THz generation by DFG was demonstrated in other nonlinear optical materials: both collinear (forward and backward) and noncollinear phase matching was used to generate broadly tunable, 20–190 cm^{-1} (0.6–5.7 THz), output in $LiNbO_3$ [9]. THz DFG was achieved with collinear phase-matching in birefringent crystals of ZGP [10, 11] and GaSe [12], and with noncollinear phase matching in cubic zinc blende structure crystals of GaAs [13, 14] and GaP [15], as well as with collinear phase-matching in GaP [16].

Guided-wave interactions between optical and THz waves can confine radiation to transverse dimensions on the order of the THz wavelength. Since DFG THz efficiency depends on pump power density, it can be enhanced in waveguides, thus lifting the tradeoff between confinement and diffraction. In addition, DFG phase matching in a THz waveguide made of nonlinear material can be achieved with optically isotropic nonlinear materials like GaAs, due to the waveguide dispersion added to the bulk dispersion of a crystal, thanks to the anomalous dispersion of those materials in the THz region. Planar GaAs waveguides (170 and 75-μm thick) were used in [17] to generate 0.5 and 1.2 THz radiation with ∼ mW peak power, by mixing outputs of two Q-switched CO_2 lasers.

Alternatively, broadly tunable (0.3–3 THz) quasi-monochromatic THz radiation can be produced through THz-wave parametric oscillation in bulk $LiNbO_3$ crystal with a single fixed-frequency optical pump [18–20]. In this case, phase matching is achieved through noncollinear three-wave interaction; the pump and the OPO resonating wave are in this case in the near infrared, while the outcoupled non-resonant wave is the THz beam.

2.2. Optical rectification (OR)

In optical rectification, THz output is produced in a nonlinear medium via difference-frequency mixing between Fourier components of the same optical pulse. First demonstrated with picosecond pulses in $LiNbO_3$ [21, 22], and ZnTe, ZnSe, CdS and quartz [21] crystals, this technique was later extended to femtosecond laser pulses [23] which made it possible to generate much broader bandwidths in terahertz region [24]. Typically, to generate broadband THz transients via optical rectification, thin (∼1 mm or less) electro-optic crystals are used, because of constraints, associated with the mismatch between optical group and terahertz phase velocities, as well as high absorption in conventional crystals ($LiNbO_3$, ZnTe) at THz frequencies. Optical rectification was also demonstrated in zinc-blende GaAs [25, 26] and GaP [27] crystals, which have intrinsically much smaller THz absorption. In the latter case, GaP was collinearly pumped by an ultrafast ($\tau \sim 210$ fs) Yb-doped fiber laser operating at 1.055 μm. A 120-MHz-repetition-rate pulse train of single-cycle THz radiation with 6.5 μW average power was generated using 10 W of laser pump [27]. Optical-to-THz conversion efficiencies in optical rectification are typically in the range 10^{-6}–10^{-9} [5]. However, recently OR conversion efficiency of $\sim 5\times10^{-4}$ was demonstrated in $LiNbO_3$ by tilting the intensity front of a femtosecond (fs) 800 nm pump pulse to match the phonon-polariton phase velocity (at THz frequencies) to the group velocity of the pump pulses in $LiNbO_3$ crystal. The authors generated near single-cycle pulses with an energy per pulse of 240 nJ [28] and 10 μJ (100 μW average power) [29]. In the latter case, energetic (20 mJ) fs laser pulses at 10 Hz repetition rate were used as pump.

2.3. Quasi-phase-matched interactions applied to THz generation

Crystals with periodic variation of the $\chi^{(2)}$ nonlinear coefficient, can solve the problem of k-vector conservation in optical-to-THz conversion process, via quasi-phase matching (QPM). In the case of optical rectification, on the other hand, QPM crystals increase effective length of collinear interaction by eliminating destructive interference due to velocity mismatch between optical and THz waves. Optical rectification in a QPM crystal was first demonstrated

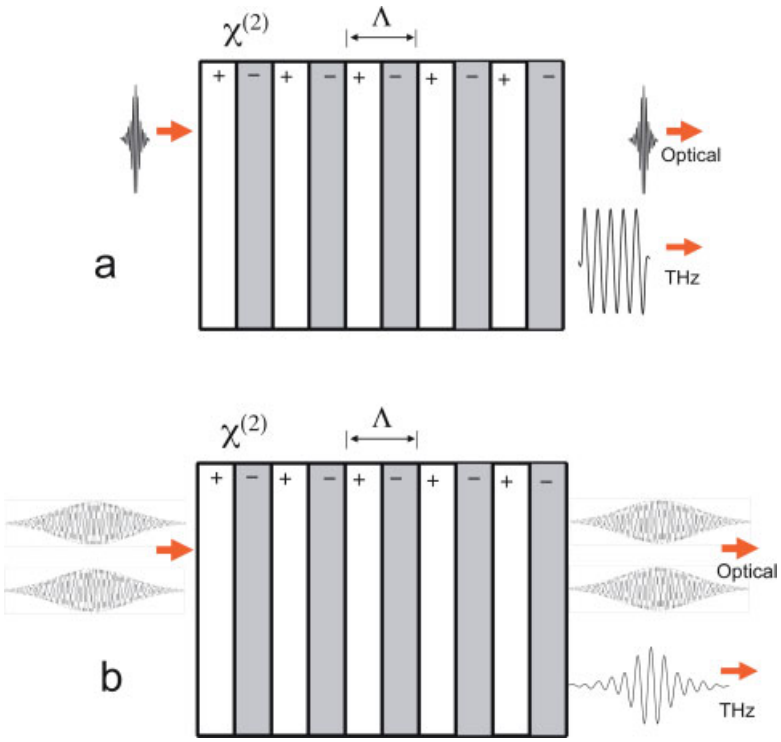

Figure 1 Schematic illustration of collinear THz-wave generation in a nonlinear crystal with periodically inverted sign of $\chi^{(2)}$. (a) Optical rectification with femtosecond pulses, (b) difference frequency generation with two picosecond pulses ($\Omega = \omega_3 - \omega_2$).

in periodically-poled lithium niobate (PPLN) [30]. The authors attained narrow-band THz generation by using femtosecond pulses at 800 nm and PPLN crystal with different QPM periods and achieved $\sim 10^{-5}$ conversion efficiency. PPLN was cryogenically cooled (T = 18 K) to reduce THz absorption. In contrast to velocity-matched single-cycle OR, optical rectification with QPM crystals gives rise to a multi-cycle narrow-band terahertz radiation with the center frequency

$$\Omega_0 = 2\pi c/\Lambda\Delta n \tag{1}$$

and spectral width corresponding to the QPM acceptance bandwidth

$$\Delta\Omega_{\mathrm{THz}} = 2\pi c/L\Delta n \tag{2}$$

where Λ is QPM period and $\Delta n = n_{\mathrm{THz}} - n_{\mathrm{g,opt}}$ is a mismatch between the THz phase (n_{THz}) and optical group ($n_{\mathrm{g,opt}}$) indices. Each inverted domain of a QPM nonlinear crystal contributes a half-cycle of the THz pulse and thus the THz wave packet has as many oscillation cycles as the number of QPM periods over the length of the crystal (Fig. 1). Also, PPLN was used in surface emitting geometries for THz generation using both OR (fs pulses) [31] and DFG (ps pulses) [32]. Lately, THz-wave generation was demonstrated in periodically-inverted GaP [33] and GaAs [34, 35]. In fact, III-V semiconductors are very attractive for QPM THz-wave generation because of several appealing properties, namely (i) small THz absorption coefficient (smaller by an order of magnitude than in commonly used EO crystals: lithium niobate, ZnTe, CdTe), (ii) large coherence length due to small mismatch between the optical group and THz phase velocities, and (iii) high thermal conductivity. In [33], THz-waves were obtained by DFG in a periodically-inverted GaP stack, produced by direct-wafer-bonding technique, and the GaP crystal was pumped with 10-nanosecond pulses near 1.55 µm.

Thus, optical THz generation in nonlinear crystals provides a variety of methods to produce THz output with an average power from nW to mW, and peak power up to megawatts. For example, single-cycle THz pulses with peak power of 5 MW were demonstrated by OR in $LiNbO_3$ [29], and sub-ns pulses with 2 MW peak power (at 1 THz) – by noncollinear DFG in GaAs, using 250-ps CO_2 laser pulses [36].

3. Theoretical limits of optical-to-THz conversion in QPM crystals

As in any $\chi^{(2)}$ parametric down-conversion process, optical-to-THz conversion efficiency scales as Ω^2, and as Ω^3, in the case of tightly focused beams [37, 38]. In particular, for the plane-wave DFG with long pulses [37]:

$$\eta_{\mathrm{THz}} = \frac{2\Omega^2 d_{\mathrm{eff}}^2 L^2}{\varepsilon_0 c^3 n_{\mathrm{opt}}^2 n_{\mathrm{THz}}} I_{\mathrm{opt}} \tag{3}$$

where η_{THz} is optical-to-THz conversion efficiency by intensity, Ω is the angular terahertz frequency, d_{eff} is the effective nonlinear optical coefficient, L is the length of the crystal, I_{opt} is the optical intensity, ε_0 is the permittivity of free space, c is the speed of light, n_{opt} is the optical refractive index, and n_{THz} is the THz refractive index. Because

of Ω^2 (or Ω^3) term, THz conversion efficiency is intrinsically low, as compared to the case of generating near- or mid-infrared radiation with the same technique; to achieve close to unity photon conversion efficiency in DFG process at 1–2 THz, one needs optical pump intensity on the order of 1 GW/cm^2 for both GaAs and $LiNbO_3$, provided that the interaction length is close to the inverse THz absorption coefficient. Moreover, very large Stokes shift imposes limitations on maximum conversion efficiency which can be achieved even if 100% photon conversion is reached.

3.1. Long pump pulses

At a given pump power, the maximum THz efficiency in a collinear DFG can be achieved with tightly focused beams (approximately confocal with respect to the THz wave). In this case, for sufficiently long pulses (ns to CW), optical-to-THz conversion efficiency scales [38] as $\eta_{THz} \sim P_{\rm opt}\Omega^3(d^2_{\rm eff}/n^2_{\rm opt})L \sim P_{\rm opt}\Omega^3(d^2_{\rm eff}/n^2_{\rm opt})/\alpha_{\rm THz}$, were $P_{\rm opt}$ is the optical pump power; we also assumed that the optimal L is on the order of $1/\alpha_{\rm THz}$, where $\alpha_{\rm THz}$ is THz power absorption coefficient (THz absorption usually dominates over optical absorption). Thus, we can introduce a figure of merit for long pulses as:

$$\mathrm{FOM}_1 = (d^2_{\rm eff}/n^2_{\rm opt})/\alpha_{\rm THz}\,. \qquad (4)$$

3.2. Quasi phase-matched OR and DFG with short pulses

Parametric frequency conversion is intensity-dependent and it might seem that, from the viewpoint of achieving high optical-to-THz efficiency, OR is more attractive than DFG, because of access to higher peak powers with fs pulses. It appears, that in a QPM case, for sufficiently short ($\tau\Omega$ <1) fs optical pulses, THz conversion efficiency in OR scales with the pulse fluence, not intensity [38]. The physical reason is that in a QPM crystal, fs pulse interacts coherently with the THz wave only over the temporal walk-off length, associated with the difference in optical group and terahertz phase velocities,$l_w \sim c\tau/\Delta n << L$ (here c is the speed of light, τ – pulse length); hence, shortening the pulse increases the peak intensity but simultaneously decreases l_w. Furthermore, in the case of mixing two ps pulses ($\tau\Omega$ >>1), with pulse durations such that the temporal walk-off length l_w is smaller than the length of the crystal, again, conversion efficiency is *fluence*-, not intensity-dependent, and has the same scaling factor as in the case of OR with femtosecond pulses. In this event, for both OR and DFG (with optimally focused beams), $\eta_{\rm THz}$ scales with *pulse energy* $U_{\rm opt}$ as $\eta_{THz} \sim U_{\rm opt}\Omega^3(d^2_{\rm eff}/n^2_{\rm opt})/\Delta n$, and a figure of merit for energy conversion efficiency for short pulses appears as:

$$\mathrm{FOM}_2 = (d^2_{\rm eff}/n^2_{\rm opt})/\Delta n\,. \qquad (5)$$

As calculations show [38], for QPM GaAs, $\eta_{\rm THz}$ ~0.1% per μJ at 1–2 THz, for both fs and ps pulses with optimized pulsewidths.

3.3. Kerr-limited interactions

In the previous example, conversion efficiency did not depend on crystal length, because we assumed that for shorter crystals we apply stronger focusing. This is true when pump intensities are moderate and we neglect high-order nonlinear effects, such as two- and three-photon absorption, and nonlinear refraction. Assuming that the pump wavelength is such that there is no two-photon absorption, and three- and higher photon-number absorption negligible, we conclude that the limiting factor is the nonlinear refraction (Kerr effect). To avoid self-focusing and self-phase modulation, pump intensity $I_{\rm opt}$ should be kept low enough to have nonlinear phase in the optical beam center to be $\Delta\varphi = 2\pi/\lambda_{\rm opt}\cdot n_2 I_{\rm opt}\cdot L < 1$ rad, where $\lambda_{\rm opt}$ is the optical wavelength and n_2 is the index of nonlinear refraction (by intensity). In this case, it is advantageous to use longer crystals ($L \sim 1/\alpha_{\rm THz}$); maximum THz conversion efficiency scales as $\lambda_{\rm opt}(d^2_{\rm eff}/n^2_{\rm opt}n_{\rm THz})L/n_2 \sim \lambda_{\rm opt}(d^2_{\rm eff}/n^2_{\rm opt}n_{\rm THz})/\alpha_{\rm THz}n_2$. Then, a figure of merit for Kerr-limited conversion is:

$$\mathrm{FOM}_3 = \lambda_{\rm opt}d^2_{\rm eff}/(n^2_{\rm opt}n_{\rm THz}\alpha_{\rm THz}n_2)\,. \qquad (6)$$

4. Comparison of nonlinear crystals for THz generation

4.1. Linear properties

Many nonlinear optical materials are relatively transparent at THz frequencies below lowest phonon resonance (e. g. at 8 THz for GaAs and 5 THz for $LiNbO_3$) and their absorption monotonically decreases with decreasing frequency. Absorption can be affected by free carriers, but in high resistivity materials (e. g. GaAs), the carrier density can be made extremely low and not contribute to absorption. Some weak features at low frequencies are due to multiphonon processes involving optical and acoustic phonons. Fig. 2 shows THz power absorption coefficient for seven nonlinear crystals at room temperature. Most of the data are based on recent measurements. One can see that GaAs, GaP and ZGP ($ZnGeP_2$) show best THz transparency below 4 THz.

4.2. Nonlinear properties

For THz frequencies well below phonon resonances, the effective nonlinear coefficient d_{jkl} for DFG and OR is nearly constant and is derived from the linear electro-optic coefficient, r, using the relation [42]: $d_{jkl} = -n^4/(4r_{jlk})$, where n is the optical refractive index. For a number of

Table 1 Linear, nonlinear optical properties, and figures of merit (normalized to $LiNbO_3$) of crystals, transparent in the 0–4 THz range and most widely used for optical THz generation.

Crystal	GaAs	GaP	ZGP	GaSe	ZnTe	$LiNbO_3$	$LiTaO_3$
Optical wavelength (μm)	2.1	1.06	2.1	1.06	0.8	1.06	1.06
Optical ref. index	3.33	3.11	3.15	2.8	2.85	2.16	2.14
THz ref. index	3.6	3.31	3.37	3.26	3.2	5.2	6.5
$\Delta n = n_{\mathrm{THz}} - n_{\mathrm{g,opt}}$	0.18	~ 0	0.17	0.34	~ 0	3.0	4.32
THz absorption at 1–2 THz, cm^{-1}	1	3.3	1	2.5	9.9	21.7	95
Electro-optic coefficient, pm/V [43]	$r_{41} = 1.5$	$r_{41} = 0.94$	$r_{41} = 1.6$	$r_{22} = 1.58$	$r_{41} = 1.4$	$r_{33} = 28$	$r_{33} = 27.7$
Nonlinear coefficient, pm/V	$d_{14} = 46.1$	$d_{14} = 21.7$	$d_{36} = 39.4$	$d_{22} = 24.3$[14]	$d_{14} = 23.1$	$d_{33} = 152.4$	$d_{33} = 145.2$
Nonlinear refractive index n_2, 10^{-15} cm^2/W @ λ (μm)	150 [44] @ 2.1	20 [45] @ 0.78	40* @ 2.1	45* @ 1.06	120 [46] @ 1.06 71 [47] @ 0.8	0.91 [48] @ 1.06	0.37* @ 1.06
FOM_1, long pulses	0.83	0.06	0.68	0.13	0.03	1	0.21
FOM_2, ultrashort pulses	0.64	1.67	0.55	0.13	0.74	1	0.64
FOM_3, Kerr-limited conversion	0.014	0.005	0.047	0.004	0.00045	1	0.416

* obtained indirectly through the bandgap scaling law of [48].

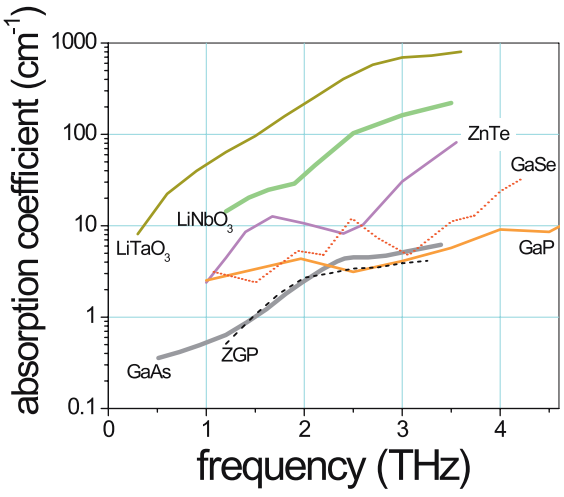

Figure 2 THz power absorption coefficients for GaAs [2], GaP [15], ZGP [39], GaSe [14], ZnTe [40], $LiNbO_3$ [41], and $LiTaO_3$ [2], measured at room temperature.

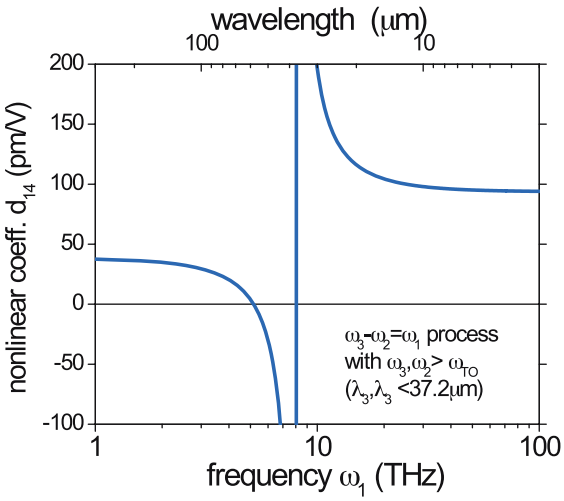

Figure 3 Nonlinear coefficient d_{14} for GaAs, as a function of THz frequency ω_1, provided that the two pump frequencies (ω_2, ω_3) are larger than the optical phonon frequency [17].

semiconductor materials, d_{jkl} is lower at THz frequencies than in the optical range, while for ferroelectric oxides like $LiNbO_3$ – there is an opposite trend. Fig. 3 shows frequency dependence of the nonlinear coefficient d_{14} for GaAs, on a broader scale of wavelengths [17].

4.3. Figures of merit

Linear and nonlinear optical properties, as well as figures of merit for the crystals, which are transparent in the 0–4 THz range, are listed in Table 1. In some crystals (ZnTe, GaP) index mismatch, Δn,can be close to zero; in this case, to calculate FOM_2, we took the walk-off length, $l_w = \sqrt{\pi} c\tau/\Delta n$ [38], to be equal (for $\tau \sim 100$ fs) to the physical length $L \sim 1/\alpha_{\mathrm{THz}}$, since l_w can not exceed L. $LiNbO_3$ crystal appears to have the largest nonlinear optical coefficient in the THz range, however GaAs has much smaller THz absorption; as a result their figures of merit FOM_1 are comparable.

5. QPM GaAs samples

Three different types of GaAs samples with periodically-inverted crystalline orientation were used for QPM THz generation: (i) diffusion-bonded GaAs (DB-GaAs) [49], produced by stacking and bonding together alternately rotated [110] GaAs plates; wafer fusion in this case creates a monolithic body with periodic change in the nonlinear

Sample	AR coated	QPM type	Aperture (mm^2)	Length (mm)	QPM period (μm)
DB-75	no	DB-GaAs	10×10	6	504
DB-77	yes	DB-GaAs	10×10	6	504
A3	no	OP-GaAs	0.4×3	3	1277
A10	no	OP-GaAs	0.4×3	10	1277
B3	no	OP-GaAs	0.4×3	3	759
B5	no	OP-GaAs	0.4×3	5	759
B10	no	OP-GaAs	0.4×3	10	759
C5	no	OP-GaAs	0.4×3	5	564
D3	no	OP-GaAs	0.4×3	3	932
3-07-1300-10A	yes	OP-GaAs	0.8×5	10	1300
OC-4-1000	yes	OC-GaAs	50×50	4	2000
OC-15-530	yes	OC-GaAs	5×5	8	1060

Table 2 Parameters of the QPM GaAs samples used in experiments.

coefficient, (ii) orientation-patterned GaAs (OP-GaAs) [50] grown by a combination of molecular beam epitaxy, photolithography, and hydride vapor phase epitaxy (HVPE), where periodic inversions of the crystallographic orientation are grown into the material, and (iii) optically–contacted GaAs (OC–GaAs) [51], which was similar to DB–GaAs since the technology involves separate plates of GaAs which are brought together, in a clean room environment, with 180^o rotation around [110] direction between neighboring plates; unlike DB-GaAs, the plates were not heated to create a uniform crystalline structure. While DB-GaAs and OC-GaAs provide large ($\sim$1 cm^2) apertures, OP-GaAs (Fig. 4) has the advantage of more reproducible technology and allows precise lithographic definition of QPM gratings; however it suffers from limited aperture (thickness) of 0.4–1 mm. Transmission loss at optical ($\lambda \sim 2\,\mu$m) frequencies was measured to be $\sim 6\%$ per cm in DB-GaAs. With the newly-grown OC-GaAs and OP-GaAs samples, transmission loss was measured to be <1 % per cm. Parameters of GaAs samples used in experiments are listed in Table 2.

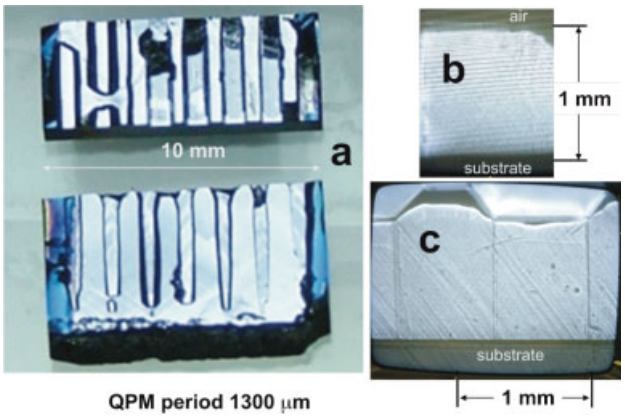

Figure 4 OP-GaAs samples for the optical THz generation with $L = 10$ mm and the QPM period of 1300 μm. (a) Top view. (b) Transmission picture of the cross section obtained with a near-infrared ($\lambda \sim 1\,\mu$m) microscope, from the polished face, as viewed by the propagating optical beam; (c) transmission picture of the grounded side face; one can see boundaries between inverted domains. The usable thickness of the samples in this case is $\sim$0.8 mm.

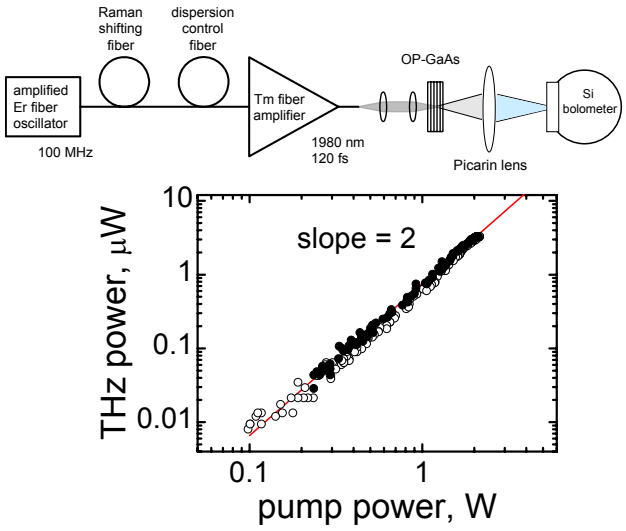

Figure 5 Schematic of the OR THz experiment with a 2-μm fiber laser. THz average power vs. laser pump power for the OP-GaAs samples A3 (filled circles) and B3 (open circles). Straight line is the best fit for the A3 data.

6. THz generation in GaAs by optical rectification

6.1. OR with fs pulses from a Tm-fiber laser at 2 μm

In order to eliminate two-photon-absorption in GaAs, one needs to use optical pumping with wavelengths $\lambda > 1.75\,\mu$m, corresponding to the photon energy which is less than half of the bandgap of GaAs. In the OR experiment, OP-GaAs crystals were pumped by a compact femtosecond fiber laser operating near 2 μm (Fig. 5). An all-fiber laser produced 120-fs pulses at 100 MHz repetition rate with the average power of 3 W (30 nJ pulse energy) at the wavelength of 1980 nm. In this fiber laser design, the output of a mode-locked Er-fiber oscillator at 1557 nm was

amplified in an Er/Yb-doped fiber amplifier, then Raman-shifted to 1980 nm, and finally amplified a large-mode-area Tm-doped fiber amplifier [35].

Two OP-GaAs samples (A3 and B3) were used, both 0.4-mm-thick and 3-mm-long. They had lithographically-defined QPM periods of 1277 µm (sample A3) and 759 µm (sample B3). The pump beam was propagating along the [110] direction of GaAs and was polarized along [111] to maximize the effective nonlinear optical coefficient. The focusing of the pump beam was optimized to produce maximum THz power with the resulting spot size ($1/e^2$ intensity radius) of w_0 = 65 µm. The generated THz beam was collimated with a Picarin plastic lens that had a focal length of 50 mm. THz power was measured with a Si bolometer operating at liquid helium temperature. A black polyethylene filter was used to block optical radiation.

Spectral properties of the generated THz radiation were measured with a Michelson interferometer. For the sample A3 the spectrum is centered at 1.78 THz and has a width of 0.3 THz, while for the sample B3 the spectrum is centered at 2.49 THz and has a width of 0.25 THz, in agreement with predicted QPM peak position and width.

Fig. 5 shows the measured THz power versus the incident optical power at 1980 nm for the samples A3 and B3, which show very similar behavior. At the highest optical power of 2.1 W available at the samples $\sim$ 3.3 µW of THz average power was obtained. The THz output power was quadratic with respect to the incident pump power and did not show any saturation effects, up to the maximum pump power of 2.1 W at the samples (peak intensity inside the samples 1.85 GW/cm^2).

6.2. OR with fs pulses from an OPA/ DFG system

Optical rectification experiments were performed in DB- and OP-GaAs using another femtosecond source, with lower repetition rate but higher peak power. Tunable pump pulses centered at 2–4.4 µm, were produced using a parametric amplifier system pumped by Ti:Sapphire pulses after a regenerative amplifier. To achieve $\lambda > 3$ µm wavelengths, an additional difference frequency generation stage was used. Typical pulse durations were $\sim$100 fs, repetition rate 1 kHz, and pulse energy up to 3 µJ [34]. GaAs samples were not AR-coated and their main parameters are listed in Table 2.

The optical pump beam with a beam size ranging between w = 300 µm and 1.5 mm, propagated along the [110] direction (or its equivalent) of GaAs. A Picarin lens was used to collect the THz radiation to the Si bolometer (4 K). To measure the spectral properties of THz radiation, a Michelson interferometer was used, composed of two 2-inch-diameter flat gold mirrors and a 25-µm-thick mylar beamsplitter (Fig. 6).

The power spectra of THz pulses were extracted in our experiment by computing the amplitudes of the Fourier transforms of Michelson interferograms. Fig. 6 shows an original interferogram and computed spectra for different samples and different pump wavelengths. THz spectra were noticeably distorted by water vapor absorption lines (also shown in Fig. 6). Experimentally observed central frequencies and bandwidths of THz pulses are in good agreement with theoretical predictions based on known GaAs dispersion relations. By changing the pump wavelength or GaAs QPM period, THz wave packets with central frequencies between 0.9 and 3 THz were generated.

The THz beam propagated collinearly with respect to the optical pump and was close to diffraction-limited (a pinhole method was used to measure the far-field THz beam size). Fig. 7 shows optical-to-terahertz conversion efficiency, η_{THz}, for samples DB-75 and A3, as a function of peak pump intensity, I_0. The pump beam size varied in this case between 300 and 810 µm. One can see that the linear dependence of η_{THz}, expected by theory, rolls off for $I_0 > 2$ GW/cm^2. This roll-off behavior was also observed at similar intensities at shorter, $\lambda \sim 2$ µm pump. The onset of saturation is most likely due to nonlinear refraction (n_2) in GaAs which induces self-phase modulation and self-focusing of the optical pulses. Indeed, if we take $n_2 \approx 1.5 \cdot 10^{-4}$ cm^2/GW for GaAs (Table 1), at I_0 = 2 GW/cm^2 and L = 6 mm, the on-axis nonlinear phase shift reaches $\sim \pi$.

In the sample DB-75, 0.66 nJ per pulse at 2.2 THz was generated at w = 300 µm, with 2.3 µJ of pump pulse energy, which corresponds to optical-to-terahertz conversion efficiency of 2.9×10^{-4}, internal efficiency 8.7×10^{-4} (the samples were un-coated), and internal photon efficiency 3.3%. These numbers are in good accord with the values calculated from [38].

7. Resonantly enhanced THz generation in GaAs using DFG

With femtosecond excitation, the limit for THz efficiency was set by parasitic high-order nonlinear effects, most likely nonlinear refraction. The optical-to-THz efficiency can be improved by using a DFG scheme with longer (ps) pulses, in the optimal case with the duration close to the walk-off time between optical and THz pulses. This condition, for a 10-mm-long GaAs and pump at $\sim$ 2 µm, corresponds to the pulse duration of 3–4 ps [38].

A near-degenerate PPLN OPO, synchronously pumped by a CW mode-locked Nd:YVO_4 laser at 1.06 µm (HighQ Laser) was built and investigated. The pump laser had repetition rate 50 MHz, pulse duration 6.5 ps, average power up to 10 W in a TEM_{00} mode. The PPLN crystal (HC Photonics), served as an OPO gain medium. It was 10-mm-long, 3-mm-wide and 1-mm-thick, had a QPM period of 14.1 µm, and was AR-coated for both 1.06 and 2.1–2.16 µm. PPLN was designed for the type-II QPM three-wave interaction (Y-YZ), so that the signal and the idler had orthogonal polarizations. The high-finesse standing-wave OPO cavity (Fig. 8) was 3-m-long and consisted of typically 7 mirrors, all of which were highly transmissive at 1.06 µm and highly reflective (>99.9%) in the vicinity of the 2.13 µm degeneracy wavelength. Mirrors M1-M2, and M7 were flat, M3-M4

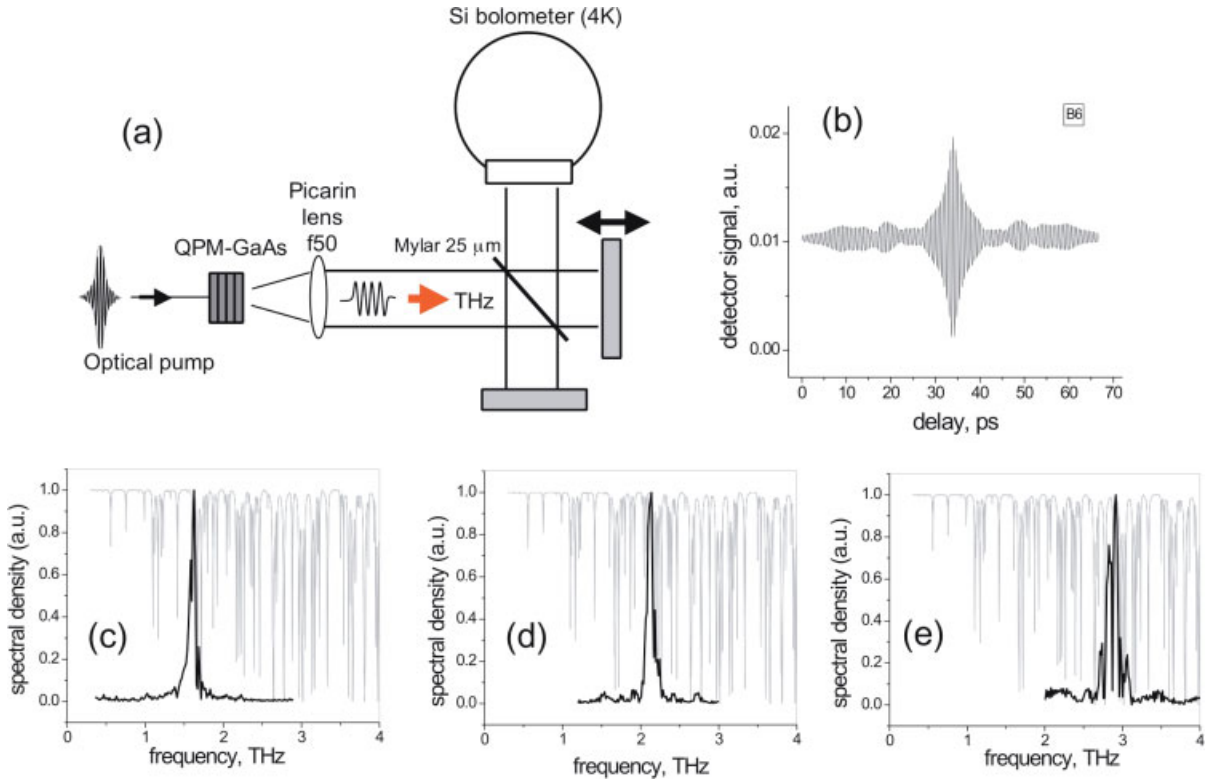

Figure 6 (a) Experimental setup for Michelson interferometry and (b) typical Michelson interferogram. Power spectra of THz pulses extracted from interferograms, for different samples and pump wavelengths: (c) B10, pump at 4.4 μm, (d) DB-75, pump at 4.4 μm, and (e) DB-75, pump at 2 μm. Shown in gray is transmission of a 20 cm path of standard air taken from the HITRAN database.

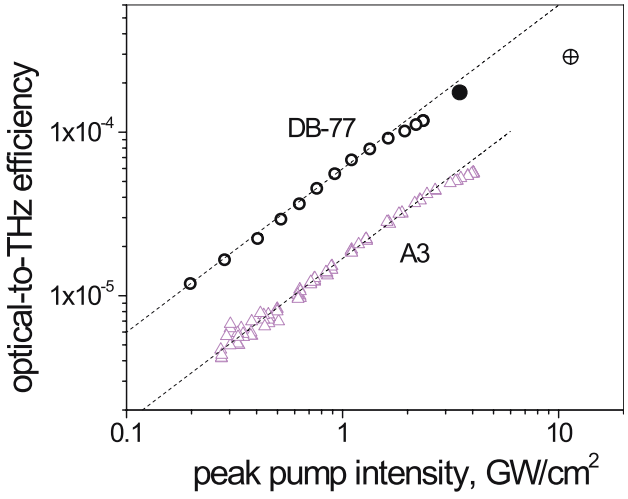

Figure 7 Optical-to-terahertz conversion efficiency as a function of peak pump intensity for the sample DB-75 (2.2 THz, circles) and A3 (1.5 THz, triangles). The pump beam size was 810 μm (open circles), 520 μm (closed circles), 590 μm (triangles), and 300 μm (crossed circles). The pump wavelength was 3.5 μm (open circles and triangles) and 4.4 μm (filled and crossed circles). Dashed lines – linear fits.

– had ROC of 200 mm, and M5-M6 – ROC of 500 mm. A thin-film polarizing beamsplitter inside the cavity served as an idler-wave outcoupler, thus the OPO in this case was singly resonant (SRO).

Insets to Fig. 8 show the signal-wave far field intensity distribution, spectral output of the OPO (signal and idler) at two different PPLN temperatures, and OPO tuning curve with respect to the PPLN temperature. The OPO linewidth, $\Delta\nu$ ~3 cm^{-1} (100 GHz), is preserved even when the OPO crosses the degeneracy point and is close to the one given by the time-bandwidth limit. In general, any frequency spacing, from 0 to 125 cm^{-1} (0–3.75 THz) between the OPO signal and the idler waves, can be achieved by changing the PPLN temperature. At the measured pump beamsize w = 31 μm and calculated signal eigenmode beamsize of w = 51 μm, the OPO threshold was ~ 1 W. At the full average pump power of 9 W available at the PPLN crystal, the idler output reached 3 W with the pump depletion of 71%. By measuring the signal-wave power leaking through one of the OPO mirrors, the intracavity resonating average signal power was measured to be as high as 120 W. Thus, there was a substantial resonant-field enhancement of the signal wave, due to low-loss cavity (the total round-trop loss was estimated to be 3%).

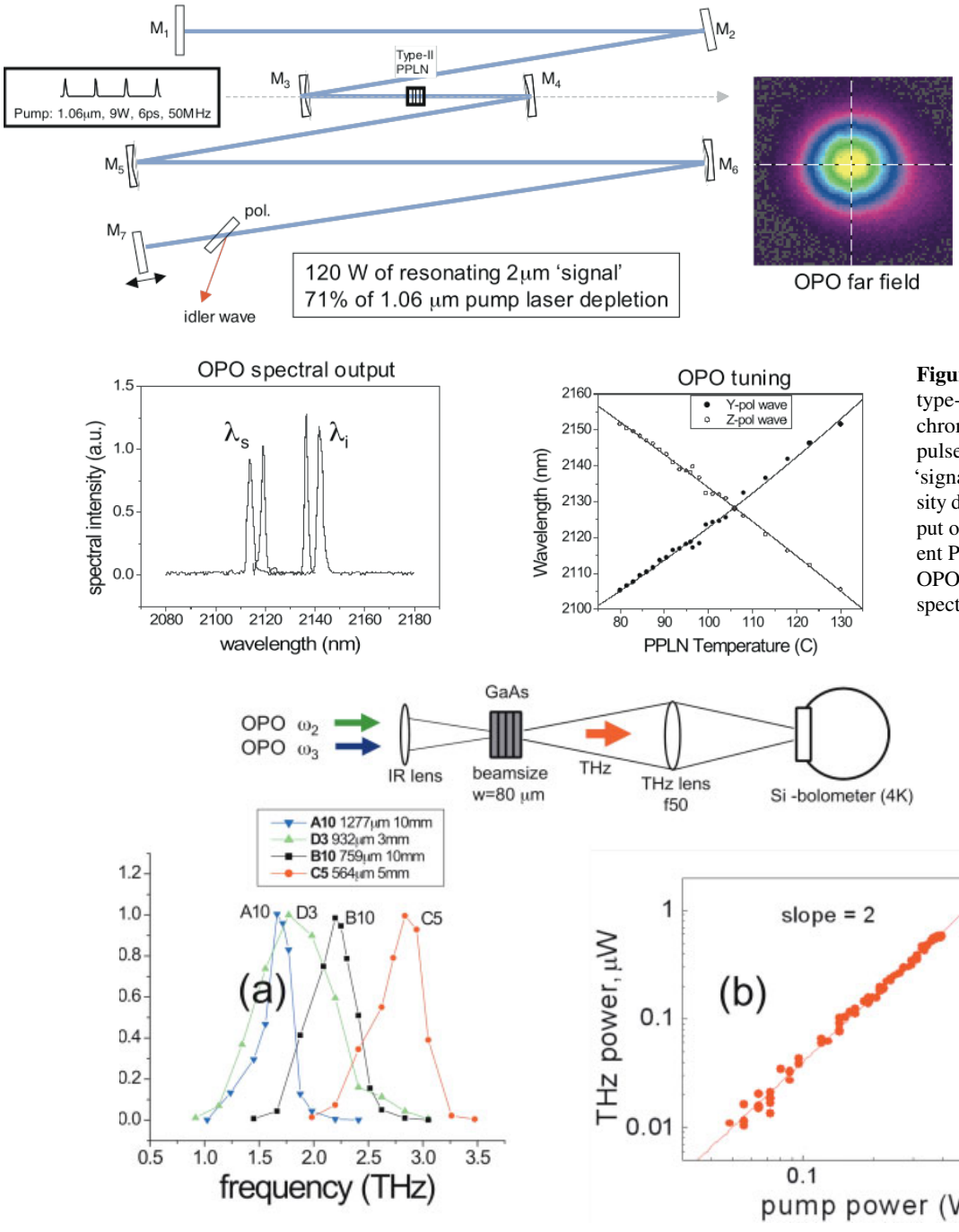

Figure 8 Near-degenerate type-II PPLN OPO, synchronously pumped by ps pulses at 1.06 μm. Insets: 'signal' wave far field intensity distribution, spectral output of the OPO at two different PPLN temperatures, and OPO tuning curve with respect to PPLN temperature.

Figure 9 (a) THz output vs. frequency in the DFG experiment outside the OPO cavity, for four OP-GaAs samples with different lengths (3–10 mm) and QPM periods (564–1277 μm). (b) THz average output power versus incoming average pump power for a 5-mm-long uncoated OP-GaAs sample (QPM period 704 μm, center frequency 2.2 THz). Straight line is the best fit.

7.1. THz generation outside the OPO cavity

In this experiment, the OPO was tuned near degeneracy and served as a dual-frequency source to produce THz output via DFG. The signal and idler beams were collinearly focused into the GaAs crystal to a beamsize of $\sim 80\,\mu$m and THz output was measured with a Si bolometer. Fig. 9a shows THz tuning curves – dependence of THz output vs. beatnote frequency (tuned by changing PPLN temperature), for 4 OP-GaAs samples (A10, D3, B10, C5 – see Table 2) with different lengths and QPM periods. THz output is maximized for each sample when the THz frequency $\Omega = \omega_3 - \omega_2$, matches the QPM condition (ω_3 and ω_2 are frequencies of the OPO signal and the idler waves corre-

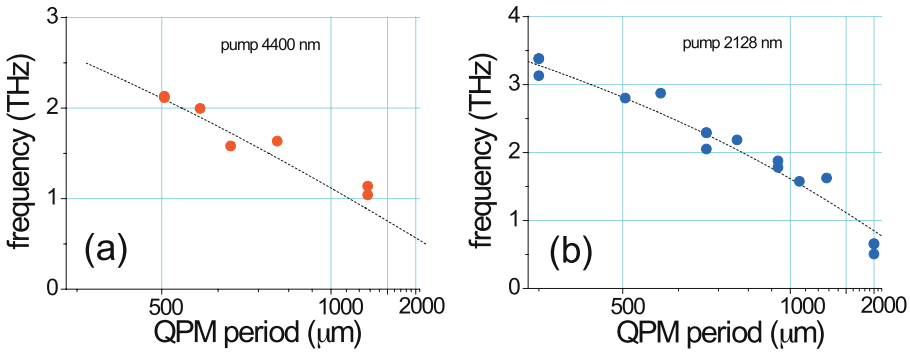

Figure 10 THz peak frequency vs. GaAs QPM period for (a) fs OR at 4400 nm pump and (b) ps DFG at 2128 nm pump. Dashed lines – calculated from known GaAs dispersion.

spondingly). Using a set of few GaAs samples, with different QPM periods, pretty broad range of THz frequencies (1–3.3 THz) can be covered. Also, one can see that longer samples give rise to narrower tuning peaks, in agreement with (2).

Fig. 9b is a log-log plot of THz average power versus average pump power for a 5-mm-long OP-GaAs sample (QPM period 704 μm, center frequency 2.2 THz). The powers at the two pump beams (OPO signal and idler) were slightly different, so geometric mean of the powers of the two beams was used as the 'pump power' on the abscissa. The best fit is a straight line with a slope of 2, which indicates that the THz output is proportional to the product of the powers of the two pump beams. The conversion efficiency was about 40% of theoretical [38]; the discrepancy can be accounted for by the beam clipping, water vapor absorption in the air at THz frequencies, and possible uncertainty in THz detector calibration. Overall, experiments with ps pulses confirm predictions of theory that THz conversion is fluence-dependent and one gets the same THz efficiency per μJ of pump pulse energy for both ps and fs pulses.

THz tuning curves (THz peak frequency vs. GaAs QPM period) obtained in this experiment are in agreement with both OR results and predictions based on known dispersion relations for GaAs (both optical and THz). Fig. 10a,b shows experimental as well as calculated tuning curves for fs OR at 4400 nm pump and extra- and intracavity ps DFG at ∼ 2128 nm pump.

7.2. Intracavity THz generation with single resonance

By placing a GaAs crystal inside the OPO cavity, one can take the advantage of resonant enhancement of pump optical power, and thus improve optical-to-THz conversion efficiency. First, an experiment with a singly resonant OPO (SRO) was performed with resonating 'signal' wave. GaAs crystal was placed near the beam waist (beamsize $w \sim 200\,\mu$m), formed by two concave mirrors with 500 mm radius of curvature inside the OPO cavity (Fig. 11a). The signal and idler beams propagated along the $[1\bar{1}0]$ crystalline direction of GaAs with polarizations aligned along [001] and [110] correspondingly. A gold-coated 90 ° -off-axis parabolic mirror (1" diameter and 2" focal length), with a 3-mm-diameter hole in its center was placed after the GaAs crystal. It fully transmitted the optical waves and allowed ∼90% outcoupling of the THz waves due to the large diffraction cone of the THz radiation.

With the AR-coated 6-mm-long DB-GaAs crystal (sample DB-77, QPM period 504 μm), 50 μW of THz output was generated at 2.8 THz. THz average power in this case was measured with a calibrated room temperature DTGS detector from Bruker (model D 201). Black polyethylene filters were used to block the 2-μm optical radiation.

When the OC-GaAs stack with comparatively large QPM period, Λ, was used, consisting of four 1-mm-thick (110) GaAs plates, three peaks of THz efficiency were observed. The center frequencies of the peaks were correspondingly at 0.66, 2.29, and 3.38 THz and their FWHM widths were 0.39, 0.32, and 0.18 THz (Fig. 12). These peaks corresponded to the 1-st, 3-rd and 5-th-order QPM in GaAs with center frequencies, $\Omega_N = 2\pi c/(\Lambda\Delta n) \times N$ ($N = 1, 3, 5$ is the QPM order), related approximately as $1 : 3 : 5$ if one neglects THz dispersion. THz output power as a function of THz frequency is shown on Fig. 12. Interestingly, the strengths of all three peaks are comparable: efficiency reduction of $1/N^2$ due to high-order QPM process [52] is offset by the Ω^2 factor which scales as N^2. Still, some difference in the peaks' strength can be explained solely by higher THz absorption at higher frequencies. Potentially, such 3-color THz source can be a useful tool for spectrally-selective THz imaging.

Fig. 13a shows the THz beam intensity profile after parabolic mirror, reconstructed from scanning knife-edge measurements. Horizontal and vertical $1/e^2$ spot sizes of 7.8 and 13.3 mm, respectively, were close to the diffraction limit. THz beam, measured in the focus of a $f = 50$ mm Picarin lens, was captured (Fig. 13b)by a room-temperature pyroelectric camera (Pyrocam III, Spiricon). The focused beam spot size is 2–3 pixels (1 pixel = $100 \times 100\,\mu$m), which again confirmed diffraction-limited performance.

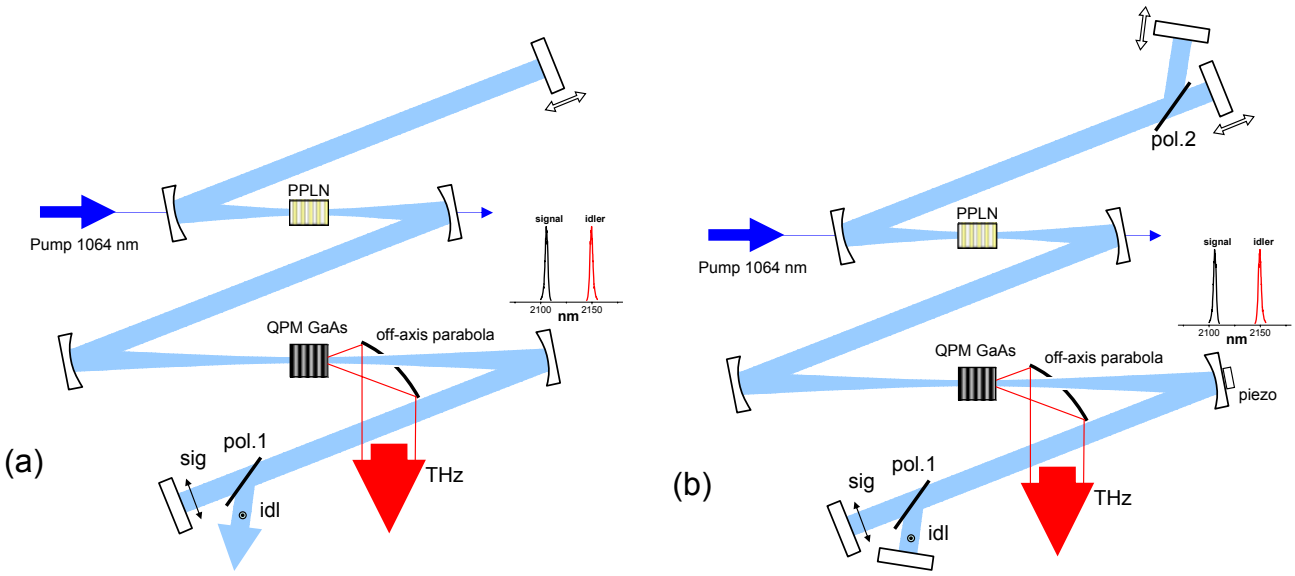

Figure 11 Setup for THz generation using GaAs inside the cavity of a near-degenerate synchronously-pumped PPLN OPO. (a) Singly-resonant OPO (SRO), (b) doubly-resonant OPO (DRO). Off-axis parabolic mirror with a hole in the center was used to extract the THz output.

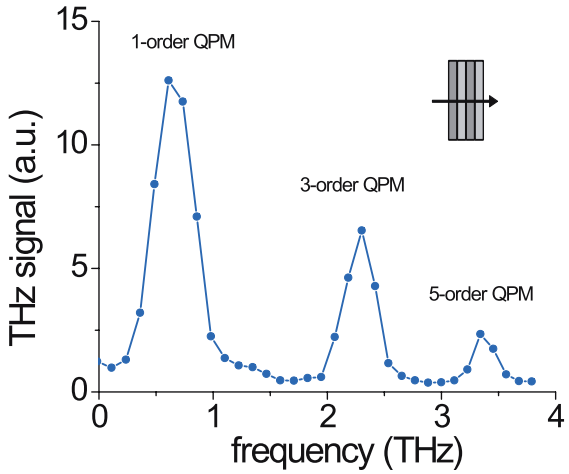

Figure 12 THz output as a function of frequency, in the case of intracavity THz generation using an OC-GaAs stack consisting of four 1-mm (110) optically-contacted plates. The peaks correspond to the 1-st, 3-rd, and 5-th-order QPM in GaAs.

7.3. Intracavity THz generation with double resonance

In a doubly resonant OPO (DRO), both optical waves are enhanced and the total THz efficiency can be further increased. Schematic of the setup for THz generation using QPM GaAs inside a DRO cavity is shown on Fig. 11b. The design of the cavity is similar to that of SRO, except for two, instead of one, thin-film polarizing beamsplitters and two separate sets of end mirrors were used to resonate simultaneously the signal and the idler waves [53].

To achieve double resonance, precise control of the two cavity lengths was needed. To accomplish that goal,

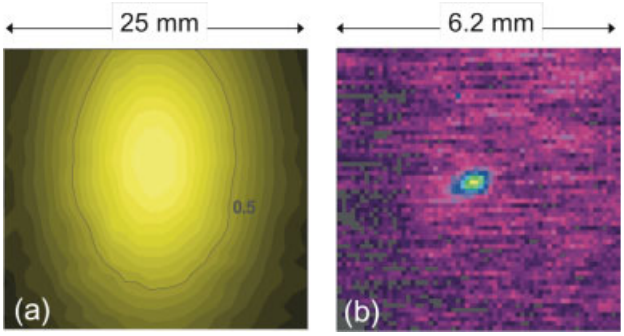

Figure 13 (a) Collimated THz-beam intensity profile reconstructed from scanning knife-edge measurements. (b) Focused (f = 50 mm lens) THz-beam intensity profile measured by a room-temperature pyroelectric camera (1 pixel = 100 × 100 µm).

the 'dither-and-lock' technique was used, involving a piezo actuator at one of the mirrors, a 2-µm photodetector and feedback electronics. Interestingly, when GaAs was placed inside the DRO cavity, self-stabilizing mechanism was observed [54], due to thermo-optic negative feedback, similar to the self-stabilizing observed earlier in a CW $AgGaS_2$ DRO [55]. In both cases of active and passive stabilization, the DRO was able to operate for $>$ 30 minutes with an excellent stability.

THz-wave generation inside DRO was achieved with all three types of QPM GaAs samples: OP-GaAs (L = 10 mm, Λ = 1300 µm, central frequency 1.27 THz), OC-GaAs (L = 8 mm, Λ = 1060 µm, 1.57 THz), and DB-GaAs (L = 6 mm, Λ = 504 µm, 2.8 THz). In the latter case, the average THz power was measured to be 1 mW, in a diffraction-limited beam, which corresponds to better than 10^{-4} optical-to-THz conversion efficiency. The resonant

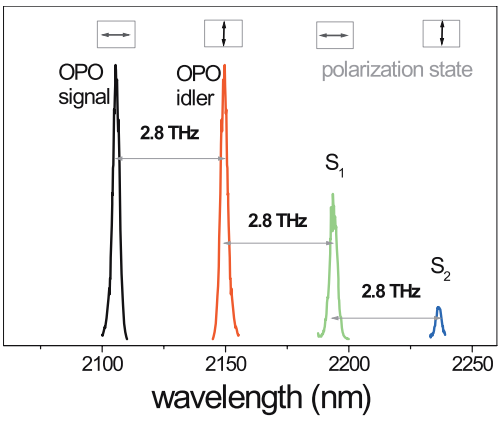

Figure 14 Spectrum of the optical radiation (not to scale vertically) in the intracavity SRO DFG experiment with the 6-mm DB-GaAs sample (center frequency 2.8 THz). In addition to the signal and the idler peaks, one can see two additional red-shifted peaks, corresponding to the 1-st and the 2-nd cascaded satellites S_1 and S_2. Polarization state of the peaks is shown on the top.

intracavity signal and idler average powers were measured to be 10.2 W and 17 W respectively.

8. Demonstration of cascaded optical-to-THz frequency conversion

The possibility of overcoming quantum-defect-related (Manley-Rowe) limitations on the efficiency of THz-wave difference frequency generation, through cascaded nonlinear optical interactions for single-pass mixing of two discrete near-infrared frequencies, was suggested by Cronin-Golomb [56]. As the pump beams run down the Stokes ladder, the number of terahertz photons should continually increase. A potential improvement by a factor of 5 was predicted for ZnTe pumped at 824 nm [56]. Cascaded down-conversion was also predicted for the case of OR, where cascading results in continuous red shift of the ultrashort pump pulse [38]. This prediction was experimentally verified quite recently – red shift of the optical pulse was observed in tilted-wavefront OR experiments in $LiNbO_3$ with high-power fs pump pulses [57], 29].

Spectrum of the optical radiation in the intracavity SRO DFG experiment with the 6-mm DB-GaAs sample and center frequency 2.8 THz is shown in Fig. 14. Idler (rather than signal) wave was made resonant in this particular SRO case. Optical radiation was extracted from the SRO cavity through one of the highly-reflecting mirrors, and analyzed using a grating monochromator. This is the first experimental demonstration of the discrete optical frequency cascading, in the DFG experiment, predicted in [56]: in addition to the signal and the idler peaks, one can see two additional red-shifted peaks, corresponding to the 1-st and the 2-nd cascaded satellites, S_1 and S_2 [54, 58]. All four peaks are spaced by the terahertz frequency (2.8 THz). Measured polarization states of the peaks are shown on the top of Fig. 14 and agree with selection rules, stating that polarizations of the neighboring peaks should be orthogonal.

The number of cascading cycles depends on the DFG pump acceptance bandwidth and on THz frequency. It can be on the order of 10 for 2-μm pump, 10-mm-long GaAs, and terahertz frequency of 1–2 THz. Potentially, THz conversion efficiency can significantly surpass the Manley-Rowe limit.

9. Conclusion

Periodically-inverted GaAs shows great promise for efficient generation of frequency-tunable narrow-bandwidth (∼ 100 GHz) THz wave packets via parametric down-conversion in the whole range from 0.5 to 3.5 THz. Both femtosecond (OR) and picosecond (DFG) optical pulses can be used as a pump. Intracavity THz wave generation with resonant enhancement of both optical waves seems to be the most efficient way of producing THz output. When GaAs was placed inside the cavity of a picosecond near-degenerate doubly-resonant OPO, 1 mW of average THz output power was achieved. With reduced intracavity losses which can be attained by lowering optical losses in QPM GaAs, as well as by switching from the linear to the ring cavity (see abstract illustration for the conceptual design), much higher THz output can be achieved. Furthermore, by allowing Stokes-shifted cascaded waves to resonate along with the signal and the idler wave (which can be achieved by special design of cavity mirrors and by compensation of the 2-nd and 3-rd order group velocity dispersion), the whole system can be scalable to 100 mW. It was difficult to make side-by-side comparison of three types of QPM GaAs samples, because of a very limited variety of QPM periods and lengths. However, there are indications that they demonstrate similar performance at similar conditions. Although OP-GaAs samples have insufficient thickness, resulting in some THz beam clipping, most likely that the OP-GaAs will be work-horse of future applications because of reproducible technology and precision of definition of QPM periods; for example, exotic gratings with aperiodic or 'fanned-out' structures can be easily created.

Acknowledgements I would like to acknowledge my collaborators at Stanford: Joe Schaar, Paulina Kuo, Xiaojun Yu, Dmitri Simanovskii, Martin Fejer, and James Harris. Also special thanks to Vladimir Kozlov and Walter Hurlbut from Microtech Instruments, Yun-Shik Lee from Oregon State University, Gennady Imeshev and Martin Fermann from IMRA America, and David Bliss and Candace Lynch from AFRL at Hanscom, MA. This work was sponsored by DARPA under AFOSR Grant FA9550-04-1-0465.

Konstantin Vodopyanov obtained his Masters degree from Moscow Phys-Tech and accomplished his PhD in 1983 in the Oscillations Lab of Lebedev Physical Institute, led by Nobel Prize winner Alexander Prokhorov. He was an assistant professor at Moscow Phys-Tech (1985–90), Alexander-von-Humboldt Fellow at the University of Bayreuth, Germany (1990–92), and a Royal Society Fellow and lecturer at Imperial College, London, UK (1992–98). He was awarded a DSc degree (Habilitation) by General Physics Institute, Moscow in 1993. In 1998, he moved to the United States and became head of the laser group at Inrad, Inc., NJ (1998–2000), and later director of mid-IR systems at Picarro, Inc.,CA (2000–2003). In 2003 he returned to Academia and is now at E. L. Ginzton Lab at Stanford University. K. Vodopyanov was elected a Fellow of the UK Institute of Physics (1997) and a Fellow of the Optical Society of America (1998). He is member of program committees for several major laser conferences and was elected Program Chair for CLEO'2008 and General Chair for 2010. His present research interests include laser interaction with matter, laser spectroscopy, nonlinear optics, mid-IR and terahertz-wave generation using micro-and nanostructured materials, as well as spectrally-resolved atomic force microscopy.

References

[1] M. Tonouchi, Cutting-edge terahertz technology, Nature Photonics **1**, 97 (2007).

[2] A. Mayer and F. Keilmann, Far-infrared nonlinear optics. I. $\chi^{(2)}$ near ionic resonance, Phys. Rev. B **33**, 6954 (1986).

[3] R. R. Jones, D. You, and P. H. Bucksbaum, Ionization of Rydberg atoms by subpicosecond half-cycle electromagnetic pulses, Phys. Rev. Lett. **70**, 1236 (1993).

[4] P. Gaal, K. Reimann, M. Woerner, T. Elsaesser, R. Hey, and K. H. Ploog, Nonlinear Terahertz Response of n-Type GaAs, Phys. Rev. Lett. **96**, 187402 (2006).

[5] P. H. Siegel, Terahertz technology, IEEE Trans. Microw. Theory Tech. (USA) **50**, 910 (2002).

[6] D. J. Cook and R. M. Hochstrasser, Intense terahertz pulses by four-wave rectification in air, Opt. Lett. **25**, 1210 (2000).

[7] T. Bartel, P. Gaal, K. Reimann, M. Woerner, and T. Elsaesser, Generation of single-cycle THz transients with high electric-field amplitudes, Opt. Lett. **30**, 2805 (2005).

[8] F. Zernike, Jr. and P. R. Berman, Generation of far infrared as a difference frequency, Phys. Rev. Lett. **15**, 999 (1965).

[9] K. H. Yang, J. R. Morris, P. L. Richards, and Y. R. Shen, Phase-matched far-infrared generation by optical mixing of dye laser beams, Appl. Phys. Lett. **23**, 669 (1973).

[10] G. D. Boyd, T. J. Bridges, and C. K. N. Patel, Phase-matched submillimeter wave generation by difference-frequency mixing in $ZnGeP_2$, Appl. Phys. Lett. **21**, 553 (1972).

[11] W. Shi, Y. J. Ding, and P. G. Schunemann, Coherent terahertz waves based on difference-frequency generation in an annealed zinc-germanium phosphide crystal: improvements on tuning ranges and peak powers, Opt. Commun. **233**, 183 (2004).

[12] W. Shi, Y. J. Ding, N. Fernelius, and K. Vodopyanov, Efficient, tunable, and coherent 0.18–5.27-THz source based on GaSe crystal, Opt. Lett. **27**, 1454 (2002).

[13] B. Lax, R. L. Aggarwal, and G. Favrot, Far-infrared step-tunable coherent radiation source: 70 µm to 2 mm, Appl. Phys. Lett. **23**, 679–681 (1973).

[14] S. Ya. Tochitsky, C. Sung, S. E. Trubnick, C. Joshi, and K. L. Vodopyanov, High-power tunable, 0.5–3 THz radiation source based on nonlinear difference frequency mixing of CO_2 laser lines, J. Opt. Soc. Am. B, Opt. Phys. **24**, 2509 (2007).

[15] T. Tanabe, K. Suto, J. Nishizawa, K. Saito, and T. Kimura, Tunable THz wave generation in the 3- to 7-THz region from GaP, Appl. Phys. Lett. **83**, 237 (2003).

[16] T. Taniuchi and H. Nakanishi, Continuously tunable terahertz-wave generation in GaP crystal by collinear difference frequency mixing, Electron. Lett. **40**, 327 (2004).

[17] D. E. Thompson and P. D. Coleman, Step-tunable far infrared radiation by phase matched mixing in planar-dielectric waveguides, IEEE Trans. Microw. Theory Tech. (USA) **12**, 995–1000 (1974).

[18] M. A. Piestrup, R. N. Fleming, and R. H. Pantell, Continuously tunable Submillimeter wave source, Appl. Phys. Lett. **26**, 418 (1975).

[19] K. Kawase, M. Sato, T. Taniuchi, and H. Ito, Coherent tunable THz-wave generation from LiNbO3 with monolithic grating coupler, Appl. Phys. Lett. **68**, 2483(1996).

[20] T. J. Edwards, D. Walsh, M. B. Spurr, C. F. Rae, M. H. Dunn, and P. G. Browne, Compact source of continuously and widely tunable terahertz radiation, Opt. Express **14**, 1582–4 (2006).

[21] T. Yajima and N. Takeuchi, Far-infrared difference-frequency generation by picosecond laser pulses, Jpn. J. Appl. Phys. **9**, 1361 (1970).

[22] K. H. Yang, P. L. Richards, and Y. R. Shen, Generation of far-infrared radiation by picosecond light pulses in $LiNbO_3$, Appl. Phys. Lett. **19**, 320 (1971).

[23] L. Xu, X.-C. Zhang, and D. H. Auston, Terahertz beam generation by femtosecond optical pulses in electro-optic materials, Appl. Phys. Lett. **61**, 1784(1992).

[24] B. Ferguson and X.-C. Zhang, Materials for terahertz science and technology, Nature Mater. **1**, 26 (2002).

[25] A. Rice, Y. Jin, X. F. Ma, X.-C. Zhang, D. Bliss, J. Larkin, and M. Alexander, Terahertz optical rectification from <110> zinc-blende crystals, Appl. Phys. Lett. **64**, 1324 (1994).

[26] M. Nagai, K. Tanaka, H. Ohtake, T. Bessho, T. Sugiura, T. Hirosumi, and M. Yoshida, Generation and detection of terahertz radiation by electro-optical process in GaAs using 1.56 µm fiber laser pulses, Appl. Phys. Lett. **85**, 3974 (2004).

[27] G. Chang, C. J. Divin, C.-H. Liu, S. L. Williamson, A. Galvanauskas, and T. B. Norris, Power scalable compact THz system based on an ultrafast Yb-doped fiber amplifier, Opt. Express **14**, 7909 (2006).

[28] A. Stepanov, J. Kuh, I. Kozma, E. Riedle, G. Almási, and J. Hebling, Scaling up the energy of THz pulses created by optical rectification, Opt. Express **13**, 5762 (2005).
[29] K.-L. Yeh, M. C. Hoffmann, J. Hebling, and K. A. Nelson, Generation of 10 µJ ultrashort terahertz pulses by optical rectification, Appl. Phys. Lett. **90**, 171121 (2007).
[30] Y.-S. Lee, T. Meade, V. Perlin, H. Winful, T. B. Norris, and A. Galvanauskas, Generation of narrow-band terahertz radiation via optical rectification of femtosecond pulses in periodically poled lithium niobate, Appl. Phys. Lett. **76**, 2505–2507 (2000).
[31] C. Weiss, G. Torosyan, Y. Avetisyan, and R. Beigang, Generation of tunable narrow-band surface-emitted terahertz radiation in periodically poled lithium niobate , Opt. Lett. **26**, 563 (2001).
[32] Y. Sasaki, Y. Avetisyan, H. Yokoyama, and H. Ito, Surface-emitted terahertz-wave difference frequency generation in two-dimensional periodically poled lithium niobate, Opt. Lett. **30**, 2927 (2005).
[33] I. Tomita, H. Suzuki, H. Ito, H. Takenouchi, K. Ajito, R. Rungsawang, and Y. Ueno, Terahertz-wave generation from quasi-phase-matched GaP for 1.55 µm pumping, Appl. Phys. Lett. **88**, 071118-1 (2006).
[34] K. L. Vodopyanov, M. M. Fejer, X. Yu, J. S. Harris, Y.-S. Lee, W. C. Hurlbut, V. G. Kozlov, D. Bliss, and C. Lynch, Terahertz-wave generation in quasi-phase-matched GaAs, Appl. Phys. Lett. **89**, 141119-1 (2006).
[35] G. Imeshev, M. E. Fermann, K. L. Vodopyanov, M. M. Fejer, X. Yu, J. S. Harris, D. Bliss, and C. Lynch, High-power source of THz radiation based on orientation-patterned GaAs pumped by a fiber laser, Opt. Express **14**, 4439 (2006).
[36] S. Ya. Tochitsky, J. E. Ralph, C. Sung, and C. Joshi, Generation of magawatt-power terahertz pulses by noncollinear difference-frequency mixing in GaAs, J. Appl. Phys. **98**, 026101 (2005).
[37] R. L. Aggarwal and B. Lax, Optical mixing of CO_2 lasers in the far-infrared, in: Topics in Appl. Phys. Vol. 16 "Nonlinear infrared generation", edited by Y.-R. Shen (Springer, Berlin, 1977).
[38] K. L. Vodopyanov, Optical generation of narrow-band terahertz packets in periodically inverted electro-optic crystals: conversion efficiency and optimal laser pulse format, Opt. Express **14**, 2263 (2006).
[39] Our measurements with BioRad far-infrared FTIR spectrometer.
[40] G. Gallot, J. Zhang, R. W. McGowan, T.-I. Jeon, and D. Grischkowsky, Measurements of the THz absorption and dispersion of ZnTe and their relevance to the electro-optic detection of THz radiation, Appl. Phys. Lett. **74**, 3450 (1999).
[41] J. Shikata, M. Sato, T. Taniuchi, H. Ito, and K. Kawase, Enhancement of terahertz-wave output from $LiNbO_3$ optical parametric oscillators by cryogenic cooling, Opt. Lett. **24**, 202 (1999).
[42] G. D. Boyd, T. J. Bridges, M. A. Pollack, and E. H. Turner, Microwave nonlinear susceptibilities due to electronic and ionic anharmonicities in acentric crystals, Phys. Rev. Lett. **26**, 387 (1971).
[43] D. N. Nikogosyan, Properties of Optical and Laser-Related Materials. A Handbook (Wiley, Chichester, 1997).
[44] W. C. Hurlbut, Yun-Shik Lee, K. L. Vodopyanov, P. S. Kuo, and M. M. Fejer, Multi-photon absorption and nonlinear refraction of GaAs in the mid-infrared, Opt. Lett. **32**, 668 (2007).
[45] M. Yin, X. Sun, S. H. Tang, and W. Ji, Femtosecond determination of optical nonlinearities in CdS, GaP, ZnO, ZnS, ZnSe and ZnTe, in: Proceedings of the Conference on Lasers and Electro-Optics, Pacific Rim 1999, Tech. Digest., p. 873 (1999).
[46] A. A. Said, M. Sheik-Bahae, D. J. Hagan, T. Wei, J. Wang, J. Young, and E. W. Van Stryland, Determination of bound-electronic and free-carrier nonlinearities in ZnSe, GaAs, CdTe, and ZnTe, J. Opt. Soc. Am. B, Opt. Phys. **9**, 405 (1992).
[47] W.-Q. He, C.-M. Gu, and W.-Z. Shen, Direct evidence of Kerr-like nonlinearity by femtosecond Z-scan technique, Opt. Express **14**, 5476 (2006).
[48] R. DeSalvo, A. A. Said, D. J. Hagan, E. W. Van Stryland, and M. Sheik-Bahae, Infrared to ultraviolet measurements of two-photon absorption and n_2 in wide bandgap solids, IEEE J. Quantum Electron. **32**, 1324 (1996).
[49] L. A. Gordon, G. L. Woods, R. C. Eckardt, R. K. Route, R. S. Feigelson, M. M. Fejer, and R. L. Byer, Diffusion-bonded stacked GaAs for quasi-phase-matched second-harmonic generation of a carbon dioxide laser, Electron. Lett. **29**, 1942 (1993).
[50] L. A. Eyres, P. J. Tourreau, T. J. Pinguet, C. B. Ebert, J. S. Harris, M. M. Fejer, L. Becouarn, B. Gerard, and E. Lallier, All-epitaxial fabrication of thick, orientation-patterned GaAs films for nonlinear optical frequency conversion, Appl. Phys. Lett. **79**, 904 (2001).
[51] Y.-S. Lee, W. C. Hurlbut, K. L. Vodopyanov, M. M. Fejer, and V. G. Kozlov, Generation of multicycle terahertz pulses via optical rectification in periodically inverted GaAs structures, Appl. Phys. Lett. **89**, 181104 (2006).
[52] M. M. Fejer, G. A. Magel, D. H. Jundt, and R. L. Byer, Quasi-phase-matched second harmonic generation: tuning and tolerances, IEEE J. Quantum Electron. **28**, 2631 (1992).
[53] J. E. Schaar, K. L. Vodopyanov, and M. M. Fejer, Intracavity terahertz-wave generation in a synchronously pumped optical parametric oscillator using quasi-phase-matched GaAs, Opt. Lett. **32**, 1284 (2007).
[54] J. E. Schaar, K. L. Vodopyanov, P. S. Kuo, M. M. Fejer, X. Yu, A. Lin, J. S. Harris, D. Bliss, C. Lynch, V. G. Kozlov, and W. Hurlbut, Terahertz sources based on intracavity parametric down-conversion in quasi-phase-matched gallium arsenide, submitted to IEEE J. Sel. Top. Quantum Electron.
[55] A. Douillet, J.-J. Zondy, A. Yelisseyev, S. Lobanov, and L. Isaenko, Stability and frequency tuning of thermally loaded continuous-wave $AgGaS_2$ optical parametric oscillators, J. Opt. Soc. Am. B, Opt. Phys. **16**, 1481 (1999).
[56] M. Cronin-Golomb, Cascaded nonlinear difference-frequency generation of enhanced terahertz wave production, Opt. Lett. **29**, 2046 (2004).
[57] A. G. Stepanov, A. A. Melnikov, V. O. Kompanets, and S. V. Chekalin, Spectral modification of femtosecond laser pulses in the process of highly efficient generation of terahertz radiation via optical rectification, JETP Lett. (USA) **85**, 227 (2007).
[58] J. E. Schaar, K. L. Vodopyanov, M. M. Fejer, X. Yu, J. S. Harris, C. Lynch, D. Bliss, and V. G. Kozlov, Tunable

Terahertz Generation inside a Synchronously-Pumped Optical parametric oscillator using quasi-phasematched GaAs, in: Proceedings of the Optical Terahertz Science and Technology Topical Meeting (OTST'2007), Orlando, FL, Technical Digest, paper WB7 (2007).